Evolution of Defects in the Bulk Structure of MoO_3 During the Catalytic Oxidation of Propene

Thorsten Ressler,*[a] Julia Wienold,[a] Rolf E. Jentoft,[a] and Frank Girgsdies[a]

Keywords: Molybdenum / EXAFS spectroscopy / X-ray diffraction / Heterogeneous catalysis / Oxidation

The evolution of characteristic defects in the bulk structure of MoO_3 under propene oxidation conditions was investigated by in situ X-ray absorption spectroscopy and X-ray diffraction. Under the reaction conditions employed (273 K to 773 K, and propene to oxygen ratios from 1:1 to 1:5), orthorhombic MoO_3 remains the only crystalline phase detected by XRD. The starting temperature for the reaction of propene and oxygen in the presence of MoO_3 coincides with the temperature at which reduction of MoO_3 begins in He, H_2 and propene ($\approx$ 620 K). At temperatures below 720 K, and independent of the atmosphere used, partial reduction of MoO_3 is observed resulting in the formation of "$Mo_{18}O_{52}$" type defects in the layer structure of α-MoO_3. At temperatures above 720 K, and under oxygen or in an oxidizing atmosphere, the "$Mo_{18}O_{52}$" type defects are reoxidized to MoO_3. Evidently, the catalytically active molybdenum oxide phase develops under partial oxidation conditions at temperatures below 720 K, and does not possess the undisturbed ideal layer structure of orthorhombic α-MoO_3. The results presented clearly show the necessity and the potential for bulk structural investigations of heterogeneous catalysts under the reaction conditions used. The bulk structure, and particularly the type and number of defects in the material ("real" structure) considerably affect the catalytic properties. Hence, in order to rationally design a most active heterogeneous catalyst, both the structure and reactions of the surface, and the structure, defects, and reactions of the bulk need to be known in detail, and carefully considered.

Introduction

Molybdenum trioxide, MoO_3, is an active catalyst for the oxidation of propene in the presence of gaseous dioxygen at temperatures above about 600 K. Moreover, MoO_3 constitutes a suitable three-dimensional model system for the more complex molybdenum based mixed oxide catalysts that are employed industrially for various partial oxidation reactions. Hence, the structural features and the catalytic properties of MoO_3 have been investigated in detail over the last five decades in order to reveal structure-activity relationships and to aid the rational design of improved catalyst materials.[1−4] Accordingly, the various steps of the molecular mechanism of the oxidation of propene in the presence of MoO_3 have been suggested to include adsorption of propene on the surface of the catalyst, abstraction of hydrogen, and the formation of an allylic species.[5,6] Subsequently, oxygen from the lattice of MoO_3 is incorporated in the allylic species, forming the partial oxidation product acrolein, or the total oxidation product carbon dioxide. The bulk of the metal oxide is then reoxidized by oxygen from the gas phase ("redox mechanism" or "Mars−van Krevelen mechanism").[7−9]

Although it is assumed that the lattice oxygen of MoO_3 participates in the oxidation of propene, little is known about defects in the regular layer structure of MoO_3 that may form under the reaction conditions, or about the structural properties and the role of these defects in the partial oxidation reactions proceeding on the surface of the MoO_3 catalyst. The question remains, how close is the "real" bulk structure of MoO_3 under the reaction conditions to the "ideal" structure of orthorhombic α-MoO_3?

Under propene oxidation reaction conditions, MoO_3 exhibits a slightly reduced average valence, which, according to the conventional redox mechanism, has to be attributed to different rates for the reduction and the re-oxidation of the molybdenum trioxide.[1] Since molybdenum is known to form a number of well-defined suboxides with average valences between 6.0 (MoO_3) and 4.0 (MoO_2) (i.e. $Mo_{18}O_{52}$, $Mo_{17}O_{47}$, Mo_9O_{26}, Mo_8O_{23}, Mo_5O_{14}, Mo_4O_{11}), it has been speculated that one of these suboxides constitutes the active phase in a molybdenum oxide partial oxidation catalyst. Thus, stoichiometric reduction and oxidation of various molybdenum oxides have been studied extensively in the past, with various attempts to correlate the observations made with the catalytic behavior of the materials investigated.[1] Those studies have proven extremely valu-

[a] Department of Inorganic Chemistry, Fritz-Haber-Institut der MPG,
Faradayweg 4−6, 14195 Berlin, Germany
Fax: (internat.) + 49-(0)30/8413−4405
E-mail: Ressler@fhi-berlin.mpg.de

able to elucidate the evolution of the phase composition and the bulk structure during reduction and oxidation of the molybdenum oxides, and to determine the solid-state kinetics of these reactions. Recently, we were able to show that only $Mo_{18}O_{52}$ is a possible intermediate of the reduction of MoO_3 in propene and the oxidation of MoO_2 in oxygen,[10] while none of the well-defined suboxides were detected during reduction of MoO_3 in hydrogen at temperatures below about 700 K.[11] However, the evolution of the bulk structure of MoO_3 under catalytic reaction conditions and the formation of defects have largely been neglected in the past.

Investigations of the relationships between the structure and the reactivity of a heterogeneous catalyst need to be performed in situ (i.e. under "real" reaction conditions), with simultaneous monitoring of the catalyst structure and the gas phase composition.[12] Naturally, "post mortem" investigations of catalysts at room temperature, in air or in an inert atmosphere, cannot provide unambiguous correlations between the structure and the reactivity of the solid. Only few bulk structural techniques can readily be employed to study an active heterogeneous catalyst under "real" reaction conditions at elevated temperatures ($\geq$ 473 K) and pressures ($\geq$ 1 bar). Due to the low absorbance of hard X-rays (photon energy $\geq$ 5 keV) by gases or window materials, conventional experimental set-ups for X-ray diffraction (XRD) and X-ray absorption spectroscopy (XAS) can easily be combined with suitable environmental cells for catalytic studies. In addition to steady-state investigations, both techniques permit experiments with a suitable time-resolution (approx. 1 min) to monitor the structural evolution of the bulk phases, which can be used to elucidate the solid-state kinetics of the reactions involved.[10,13,14]

XAS and XRD are complementary techniques because together they provide information on the quantitative phase composition of amorphous and crystalline phases, the short-range and long-range order structure of the phases present, the electronic structure, and the crystallite size, microstrain, and morphology. As this data is of paramount importance to reveal structure-reactivity relationships in heterogeneous catalysis, XAS and XRD have been extensively employed under these reaction conditions.[15] However, the evolution of defects in the regular bulk structure of heterogeneous catalysts, and the relationships between the "real" structure of a solid catalyst and its reactivity has received little attention. In the future, new insight into the importance of defects in the "real" structure of solid heterogeneous catalysts, for the catalytic properties of the material can be expected from time-resolved in situ bulk structural investigations.

In this work in situ XAS and XRD combined with mass spectrometry are employed to elucidate the phase compositions, and the long-range and short-range structural evolution of MoO_3 during the temperature-programmed reaction of propene and oxygen. The formation of characteristic defects in the bulk structure of MoO_3 under reaction conditions is described as a function of the reaction temperature and the reducing potential of the gas phase.

Results

In Situ XRD − Evolution of the Long-Range Structure

Figure 1 shows the evolution of XRD patterns measured during the temperature-programmed treatment of MoO_3 in helium in the temperature range 573−773 K, with a heating rate of 0.1 K/min. The onset temperature for the reduction of MoO_3 to form MoO_2 is at about 620 K. At temperatures between 620 K and 720 K only MoO_2 and MoO_3 are detected, whereas at temperatures above 720 K Mo_4O_{11} is formed from a parallel reaction of MoO_3 and MoO_2.[11]

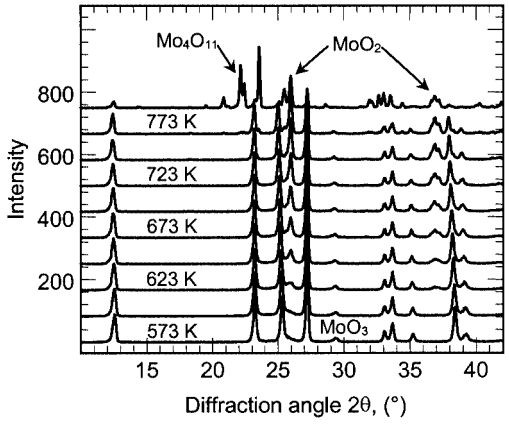

Figure 1. Evolution of XRD patterns during thermal treatment of MoO_3 in helium (573−773 K, about 0.1 K/min). The crystalline phases detected (MoO_3, MoO_2, Mo_4O_{11}) are indicated

During the temperature-programmed treatment of MoO_3 in oxygen (20% in He) in the temperature range 473−773 K with a heating rate of 0.1 K/min, MoO_3 remains the only crystalline phase detected by XRD. The evolution of ratios of integrated intensities of selected *hkl* reflections and the crystallite sizes calculated for these reflections during thermal treatment of MoO_3 in oxygen are shown in Figure 2, part (a) and (b), respectively. While the ratios shown remain nearly constant up to about 620 K, the ratios 110/101 and 020/101 increase substantially between about 620 K and about 700 K, and almost return to their original room temperature value at about 720 K. The ratio 020/110 does not change significantly in the temperature range studied. The apparent crystallite sizes calculated for the 101 and 110 reflections exhibit an increase above 673 K, while the crystallite size calculated for the 002 reflection shows a decrease between 573 K and 673 K. On cooling to room temperature, the crystallite sizes calculated for the *hkl* reflections shown are similar to those determined prior to the temperature treatment. A Williamson−Hall analysis,[16] using selected *hkl* reflections in a 2θ range from 6.0 to 55.0, only shows minor strain in the original MoO_3 materials. A certain anisotropy in the direction of the strain in the MoO_3 lattice can be deduced from the considerable scatter of the individual points in the Williamson−Hall plot obtained. However, the lack of suitable higher-order reflections did not permit a direction-dependent strain analysis. During treatment in oxygen, a slight increase in the strain occurred

at about 620 K, followed by a decrease at about 720 K (inset in Figure 2). This behavior coincides with the deviations observed in the ratios of integrated intensities [Figure 2 (a)].

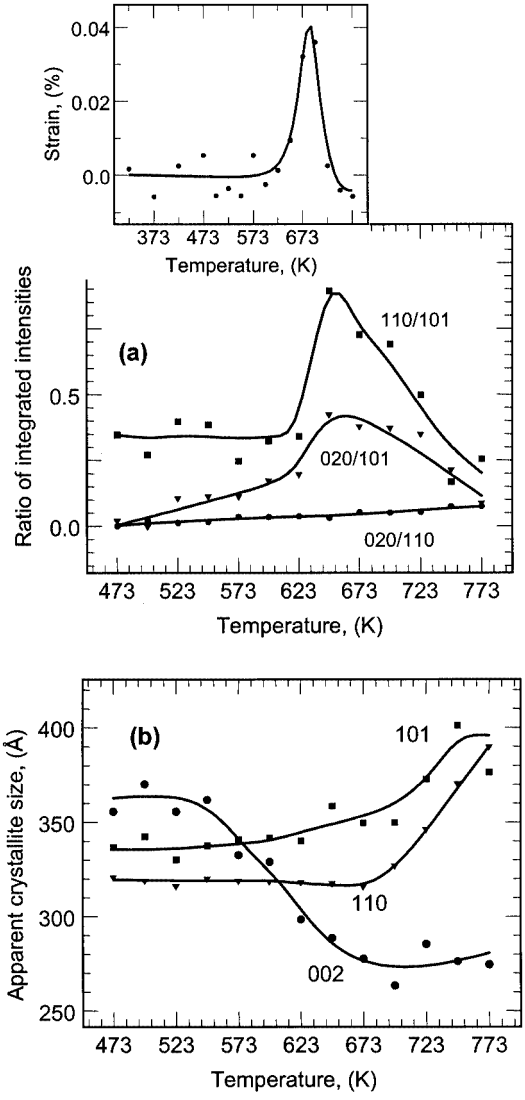

Figure 2. Evolution of ratio of integrated intensities (a) [for MoO_3 at 300 K, initial values are $A(110/101) = 4.6$, $A(020/101) = 1.9$, and $A(020/110) = 0.4$; ratios are arbitrarily displaced on y axis] and particle size (b) of selected *hkl* reflections of MoO_3 during thermal treatment of MoO_3 in oxygen (20% O_2 in He, 473−773 K, about 0.1 K/min). The inset in (a) shows the evolution of strain in the MoO_3 structure obtained from a Williamson−Hall analysis

During the temperature-programmed reaction (TPR) of propene (10 vol-%) and oxygen (10 vol-%) in the presence of MoO_3 from 473 K to 773 K, with a heating rate of 0.1 K/min, MoO_3 remains the only crystalline phase detected by XRD. The evolution of ratios of integrated intensities of selected *hkl* reflections and apparent crystallite sizes calculated for these reflections are shown in Figure 3, part (a) and part (b), respectively. Similar to the treatment in oxygen, the ratio 020/101 increases at temperatures above about 620 K, while the ratio 020/110 remains unaffected. On the other hand, the ratio 020/101 does not decrease above 720 K, but remains at a higher value. The ratio 110/101 continuously decreases between 473 K and 773 K. The apparent crystallite sizes calculated for the 110 and 002 reflections are similar to those observed during the treatment in oxygen [Figure 2, part (b)]. A Williamson−Hall analysis, using selected *hkl* reflections in the 2θ range from 6.0 to 55.0 of the diffraction patterns measured during the TPR of propene and oxygen, shows a considerable increase in the strain at temperatures above 620 K [inset in Figure 3, (a)]. This behavior coincides with the deviations observed in the ratios of integrated intensities [Figure 3, (a)].

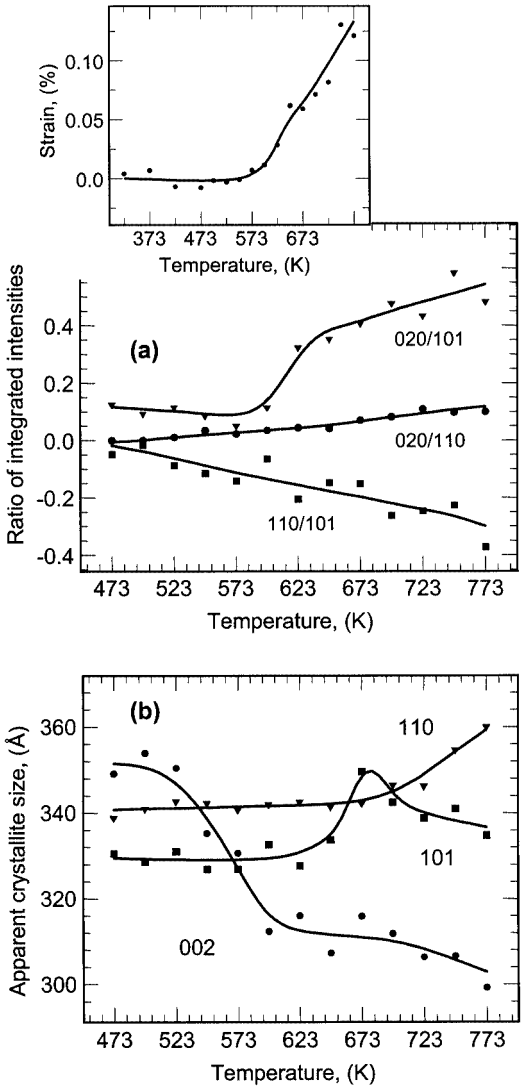

Figure 3. Evolution of ratio of integrated intensities (a) (for clarity, ratios are arbitrarily displaced on *y* axis) and particle size (b) of selected *hkl* reflections of MoO_3 during the temperature-programmed reaction of propene and oxygen (10% O_2 and 10% propene in He, 473−773 K, about 0.1 K/min). The inset in (a) shows the evolution of strain in the MoO_3 structure obtained from a Williamson−Hall analysis

In Situ XAFS − Evolution of Average Valence and Short-Range Structure

The development of the Mo-*K* edge position seen in the time-resolved XAFS spectra measured during the treatment

of MoO_3 in oxygen, and during the TPR of propene (10 vol-%) and oxygen (ratios 1:1, 1:3, and 1:5) in the presence of MoO_3 (473−773 K, 10 K/min), is depicted in Figure 4. The large number of spectra measured in the energy-dispersive mode permits reliable interpretation of small changes (< 0.1 eV) in the Mo-*K* edge position. The shift of the Mo-*K* edge position towards smaller photon energy at a temperature of about 620 K indicates the reduction of molybdenum. According to the calibration curve shown in ref.10,[10] a Mo-*K* edge shift of 0.2 eV corresponds to a difference in average valence of about 0.033. The degree of reduction under the reaction conditions for temperatures between 620 K and 720 K is related to the reducing potential of the gas phase (1:1 > 1:3 > 1:5). For the treatment of MoO_3 at temperatures above 720 K in oxygen, and in propene and oxygen with a ratio of 1:5, a shift of the Mo-*K* edge position towards higher photon energies indicates a re-oxidation of the partially reduced MoO_3. Conversely, for the reaction of propene and oxygen (ratios 1:1 and 1:3) in the presence of MoO_3, no shift of the Mo-*K* edge to higher photon energies is observed and the molybdenum oxide phase remains partially reduced at temperatures up to 773 K.

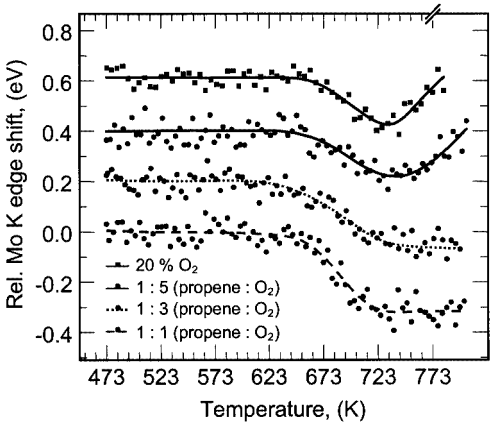

Figure 4. Evolution of Mo-*K* edge position (relative to the edge position of MoO_3, and displaced for clarity) during thermal treatment of MoO_3 in oxygen (20% in He) and during the temperature-programmed reaction of propene and oxygen in the presence of MoO_3 (10% O_2 and 10% propene in He) (473−773 K, 10 K/min, held at 773). The three different ratios of oxygen and propene employed are indicated

A principal component analysis of the XAFS spectra measured during the TPR did not afford conclusive results on the identity of the molybdenum oxide phases present. However, in addition to the temperature effect on the near-edge spectra, at least two primary components appear to be necessary to reconstruct the experimental spectra. Furthermore, the evolution of the mixing coefficients of the least important primary component shows a behavior similar to the Mo-*K* edge-shift data depicted in Figure 4.

The evolution of Mo-*K* near-edge spectra measured in the conventional XAFS mode during the TPR of propene (10%) and oxygen (10%) (300−773 K, 5 K/min) in the presence of MoO_3, together with the corresponding evolution of the average molybdenum valence, is depicted in Figure 5, part (a). Besides temperature broadening, no significant changes to the shape of the XAFS spectrum of MoO_3 occur under the reaction conditions. However, a detailed analysis of the Mo-*K* edge position again reveals a slight reduction of the molybdenum oxide at temperatures above about 620 K. Using a previously reported calibration to transform the edge-shift into average valence,[10] results in an average valence of about 5.94 for the molybdenum oxide under the reaction conditions, at temperatures above 673 K. If the type of defects formed under the TPR conditions were consistent with an "$Mo_{18}O_{52}$" type shear structure, an average valence of 5.94 would correspond to a phase composition of 75% MoO_3 and 25% $Mo_{18}O_{52}$. The evolution of the gas phase composition during the TPR of oxygen and propene in the presence of MoO_3 in a ratio of 1:1 is depicted in Figure 5, part (b). The onset temperature for the reaction is about about 620 K, producing both the partial oxidation product, acrolein and the total oxidation product, carbon dioxide. The onset temperature for the oxidation of propene was the same for all ratios of propene to oxygen measured (ratios 1:1 > 1:3 > 1:5).

Since the mass spectrometer used for the XRD and XAS experiments was not calibrated, only qualitative catalysis data can be provided. However, at 713 K, the conversion of propene in the presence of MoO_3 has been reported to be 7%, with an acrolein yield of 2%,[5] and it is assumed that the catalytic behavior of the material used here is similar. A comparison of the ratio of the ion currents of CO_2 and acrolein measured during the TPR indicates a minimum selectivity towards acrolein at about 673 K (Figure 6). This minimum selectivity is most pronounced for a ratio of propene and oxygen of 1:1.

The evolution of the Fourier-transformed Mo-*K* edge $\chi(k)$ of MoO_3 during the TPR of propene and oxygen (ratio 1:1) is depicted in Figure 7. A continuous decrease in amplitude of the higher Mo−Mo backscattering shells can be seen. As reported previously, $Mo_{18}O_{52}$ constitutes a suitable reference phase for the type of structural defects observed during reduction of MoO_3 in propene.[10] A schematic representation of the structures of orthorhombic α-MoO_3 (*Pbnm*, a = 3.936 Å, b = 13.855 Å, c = 3.696 Å)[17] and $Mo_{18}O_{52}$ ($P\bar{1}$, a = 8.145 Å, b = 11.890 Å, c = 21.230 Å, α = 102.7 °, β = 67.8 °, γ = 110.0 °)[18] is depicted in Figure 8.

The $Mo_{18}O_{52}$ structure is derived from the MoO_3 structure by crystallographic-shear operations. Hence, both contain a van der Waals gap between the individual layers, in contrast to other molybdenum oxides possessing crystallographic-shear structures such as Mo_8O_{23} and Mo_9O_{26}.[19] A comparison of the radial distribution functions of MoO_3 and $Mo_{18}O_{52}$ for a 1 nm cluster is shown in Figure 9.

The magnitude of the Fourier-transformed (FT) XAFS $\chi(k)$ of $Mo_{18}O_{52}$ will be considerably smaller than that of MoO_3 as a result of the large number of slightly different distances in the structure of $Mo_{18}O_{52}$.

In order to simulate the influence of adding certain amounts of $Mo_{18}O_{52}$ to MoO_3 on the FT[$\chi(k)$] of the re-

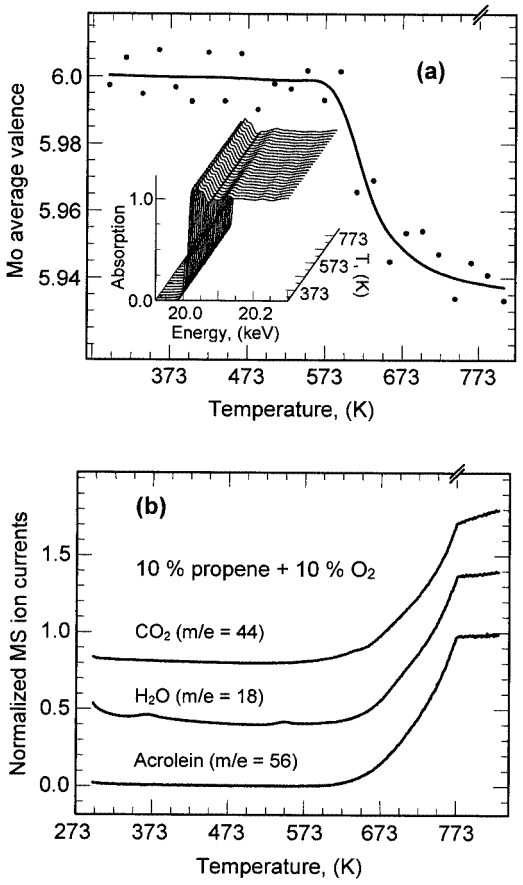

Figure 5. (a) Evolution of Mo-*K* edge position (relative to the edge position of MoO_3, and displaced for clarity) during the temperature-programmed reaction of propene and oxygen in the presence of MoO_3 (10% O_2 and 10% propene in He) (300−773 K, 5 K/min, held at 773) (inset shows evolution of XANES spectra during the TPR). (b) Evolution of the corresponding gas phase composition [CO_2 (*m/e* = 44), H_2O (*m/e* = 18), acrolein (*m/e* = 56)] during the temperature-programmed reaction of propene and oxygen

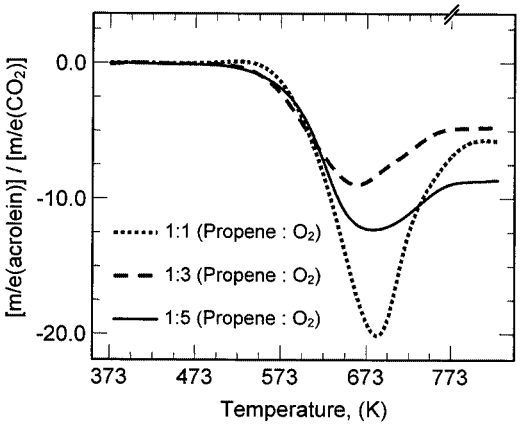

Figure 6. Ratio of the ion currents of CO_2 (*m/e* = 44) and acrolein (*m/e* = 56) measured the during temperature-programmed reaction of propene (10%) and oxygen (10% [dotted], 30% [solid], 50% [dashed]) in the presence of MoO_3 (values are displaced on the *y* axis)

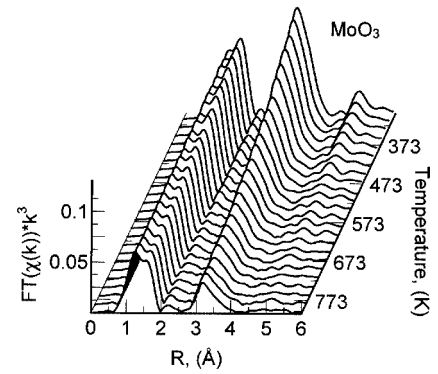

Figure 7. Evolution of Fourier-transformed $\chi(k)$ of MoO_3 during the temperature programmed reaction of propene and oxygen (10% O_2 and 10% propene in He) (300−773 K, 5 K/min, held at 773) (note inverse temperature scale) (Figure 5)

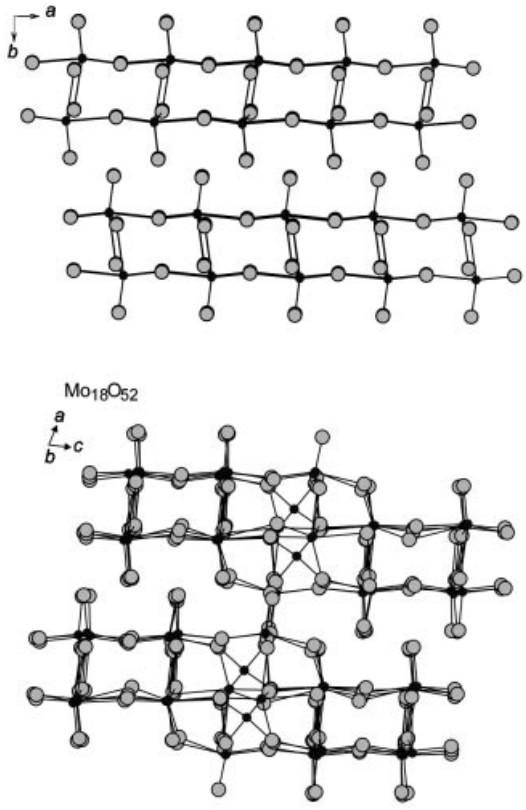

Figure 8. Schematic representations of the layer structures of MoO_3 (projection parallel to 001) and $Mo_{18}O_{52}$ (arbitrary projection for comparison with MoO_3)

sulting mixture, numerical mixtures of the experimental $\chi(k)$ of MoO_3 and $Mo_{18}O_{52}$ were calculated. The evolution of the Fourier-transformed $\chi(k)$ of these mixtures of MoO_3 and $Mo_{18}O_{52}$ is shown in Figure 10. Evidently, adding $Mo_{18}O_{52}$ to MoO_3 results in a decrease in the amplitude of all backscattering shells, in particular of the higher Mo−Mo shells. However, even for concentrations of $Mo_{18}O_{52}$ as large as 40%, the resulting FT[$\chi(k)$] strongly resembles that of MoO_3.

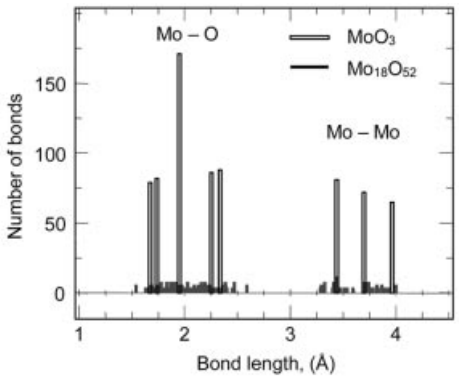

Figure 9. Comparison of radial distribution functions of MoO_3 and $Mo_{18}O_{52}$ calculated for cluster sizes of about 10 Å in both structures (≈ 330 atoms, about 670 Mo−O and Mo−Mo bonds)

Table 1. Structural parameters [coordination number (CN) and distance R of Mo−O and Mo−Mo coordination shells] of a MoO_3 model structure (*Pbnm*, a = 3.936 Å, b = 13.855 Å, c = 3.696 Å) obtained from a refinement of the model structure to the experimental XAFS functions $\chi(k)$ of MoO_3 (N_{ind} = 25, N_{free} = 13, 8 single scattering paths and 11 multiple scattering paths). Additional parameters refined are Θ(O) = 1383 K, Θ(Mo) = 442 K, E_0 = −1.5 eV (Θ: Debye temperature). The fit residual is 4.6

Shell	CN	R_{model}, (Å)	R_{MoO3}, (Å)	ΔR, (Å)	Weight (%)
Mo−O	1	1.671	1.683	0.012	71
Mo−O	1	1.735	1.710	−0.025	69
Mo−O	2	1.948	1.938	−0.01	100
Mo−O	1	2.251	2.227	−0.024	36
Mo−O	1	2.332	2.349	0.017	32
Mo−Mo	2	3.438	3.421	−0.017	91
Mo−Mo	2	3.696	3.693	−0.003	75
Mo−Mo	2	3.963	3.946	0.017	62

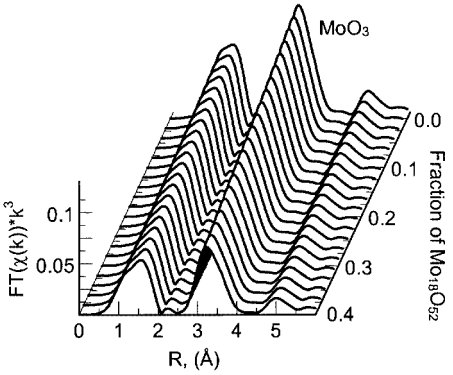

Figure 10. Evolution of Fourier-transformed $\chi(k)$ of calculated mixtures of experimental $\chi(k)$ of MoO_3 and $Mo_{18}O_{52}$, with increasing concentration of $Mo_{18}O_{52}$ (100% to 60% MoO_3)

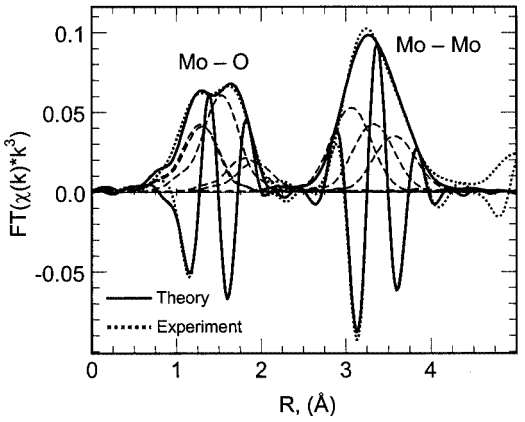

Figure 11. XAFS refinement of a theoretical Mo-K edge $\chi(k)$ (solid) to an experimental Fourier-transformed $\chi(k)$ of MoO_3 (dotted) (Table 1). The main Mo−O and Mo−Mo single-scattering paths are indicated (dashed)

The large number of different distances in the structures of MoO_3 and $Mo_{18}O_{52}$ prevents a conventional XAFS refinement of each individual distance and coordination number. Therefore, using theoretical XAFS phases and amplitudes calculated for the structure of orthorhombic α-MoO_3, structural parameters of the most prominent single-scattering and multiple-scattering paths (Table 1) in MoO_3 were refined to the calculated and measured $\chi(k)$, according to the XAFS analysis procedure described above. Thus, a detailed XAFS analysis of the set of $\chi(k)$ values of the numerical mixtures of MoO_3 and $Mo_{18}O_{52}$ (Figure 10), and the experimental spectra measured during the TPR of propene and oxygen (1:1) in the presence of MoO_3 (Figure 7) was performed to quantify the effect of the contribution of $Mo_{18}O_{52}$ on the structural parameters obtained for the MoO_3 phase. The very good agreement between refinement and experimental data that can be achieved using this fitting procedure is evident from the results of the refinement shown in Figure 11 and Table 1. For the numerical mixtures of MoO_3 and $Mo_{18}O_{52}$, the XAFS refinement procedure described above failed for concentrations of $Mo_{18}O_{52}$ larger than 27%.

The evolution of the Debye temperatures of molybdenum and oxygen backscatterers in the MoO_3 structure as a function of the concentration of $Mo_{18}O_{52}$ in the numerical mixtures and as a function of temperature during the TPR of propene and oxygen are depicted in Figure 12 (a) and Figure 12 (b), respectively. For the numerical mixtures, the Debye temperature of oxygen continuously increases for concentrations of $Mo_{18}O_{52}$ larger than 5%. The Debye temperature of molybdenum decreases linearly over the concentration range studied. For the TPR experiment, both Debye temperatures decrease almost linearly in the temperature range from 300 K to about 620 K. Above about 620 K, the Debye temperature of oxygen greatly increases, whereas the Debye temperature of molybdenum continues to decrease. For the series of XAFS spectra measured during the treatment of MoO_3 in oxygen, the increase of the Debye temperature of oxygen starting at about 620 K is followed by a decrease at temperatures above about 720 K.

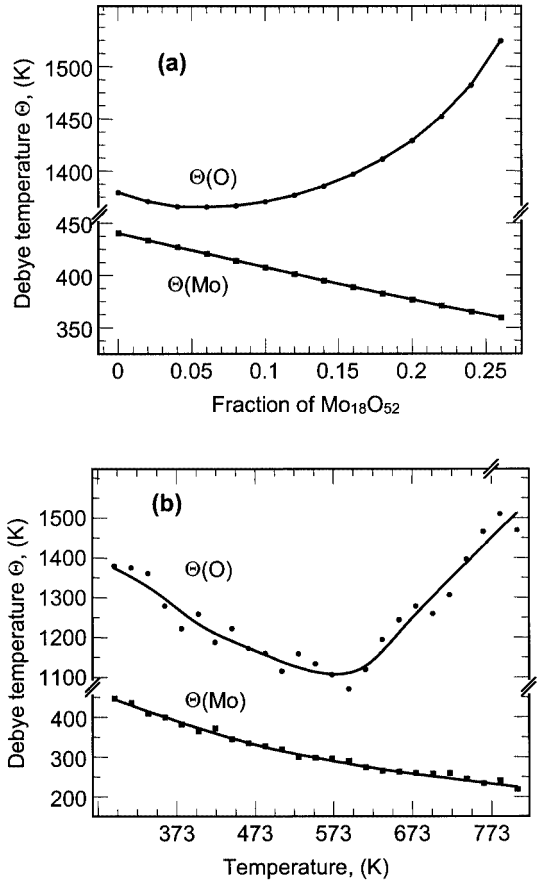

Figure 12. Evolution of Debye temperatures of molybdenum and oxygen backscatterers in the structure of MoO_3 obtained from XAFS refinement, (a) as a function of the concentration of $Mo_{18}O_{52}$ in the mixtures of MoO_3 and $Mo_{18}O_{52}$ in Figure 10 and (b) during the temperature-programmed reaction of propene and oxygen in the presence of MoO_3 (Figure 7) (10% O_2 and 10% propene in He) (300−773 K, 5 K/min, held at 773)

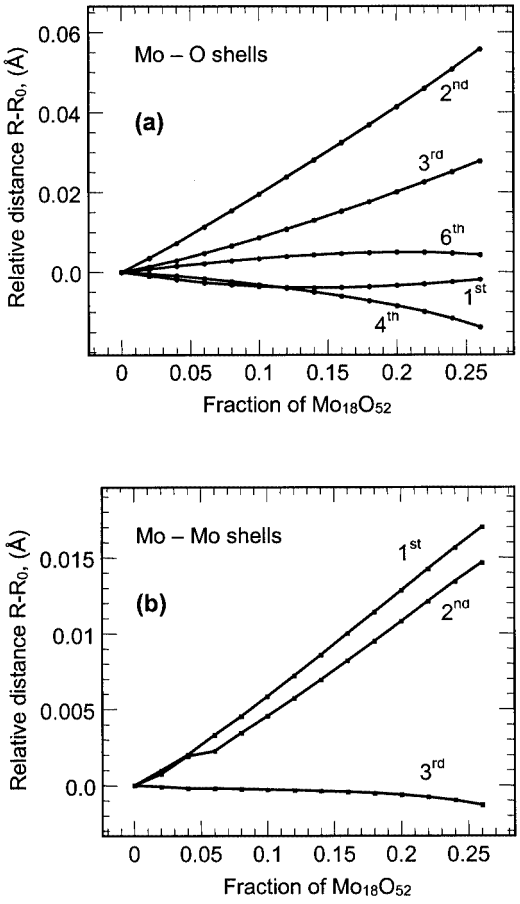

Figure 13. Evolution of relative Mo−O (a) (R_0 1st = 1.683 Å, 2nd = 1.710 Å, 3rd = 1.938 Å, 4th = 2.227 Å, 6th = 2.349 Å) and Mo−Mo (b) (R_0 1st = 3.421 Å, 2nd = 3.693 Å, 3rd = 3.946 Å) distances in the structure of MoO_3 obtained from XAFS refinement to the mixtures of MoO_3 and $Mo_{18}O_{52}$ in Figure 10

The evolution of the Mo−O and Mo−Mo distances in the first neighboring shells of the structure of MoO_3 as a function of the concentration of $Mo_{18}O_{52}$ in the numerical mixtures is displayed in Figure 13 (a and b), respectively. Figure 14 (a and b) show the evolution of Mo−O and Mo−Mo distances during the TPR of propene and oxygen. For the numerical mixtures, a pattern of increasing and decreasing distances are seen in the Mo−O and Mo−Mo distances. For the TPR experiment, there is a minor increase in the Mo−O distances in the temperature range from 300 K to about 620 K, corresponding to the anisotropic thermal expansion of MoO_3. At temperatures above about 620 K, several Mo−O distances show a strong deviation from their behavior at lower temperatures, resulting in a pattern of increasing and decreasing Mo−O distances very similar to that observed for the numerical mixtures. At temperatures above about 620 K, the Mo−Mo distances show a distinct deviation from their behavior at temperatures between 300 K and 620 K.

In order to validate the analysis procedure chosen, the suitability of other suboxides (i.e. Mo_4O_{11}, Mo_5O_{14}, and Mo_8O_{23}) to explain the deviations observed in the XAFS fit parameters was tested accordingly. Addition of more than 10% of Mo_4O_{11} and Mo_8O_{23} resulted in a considerable distortion of the FT[$\chi(k)$] and, hence, the failure of the XAFS fitting procedure used. For tetragonal Mo_5O_{14}, the radial distribution function also consists of a number of slightly different Mo−O and Mo−Mo distances. However, the XAFS parameters obtained from an analysis of numerical mixtures of the experimental $\chi(k)$ of MoO_3 and Mo_5O_{14} did not exhibit the characteristic increase in the Debye temperature of oxygen, or the characteristic pattern of increasing and decreasing Mo−O distances at temperatures above about 620 K. Hence, of the suboxides tested, only the shear-structure $Mo_{18}O_{52}$ constitutes a suitable reference for the type of defects observed in MoO_3 under reaction conditions.

Discussion

Changes in the bulk structure of an alkene oxidation catalyst under reaction conditions can occur when the lat-

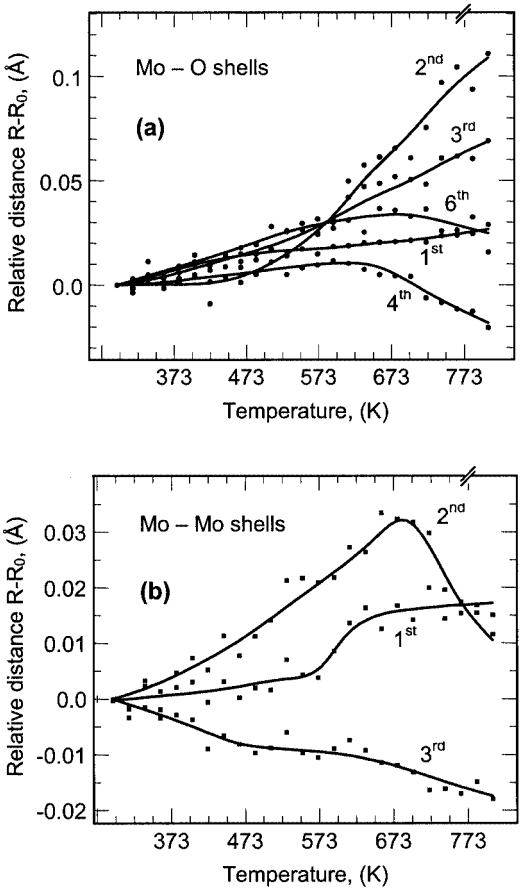

Figure 14. Evolution of relative Mo−O (a) and Mo−Mo (b) distances in the structure of MoO_3 during the temperature-programmed reaction of propene and oxygen in the presence of MoO_3 (Figure 7) (10% O_2 and 10% propene in He) (300−773 K, 5 K/min, held at 773)

tice oxygen of the catalyst participates in the oxidation of the alkene (''redox'' mechanism), and if the corresponding reduction and re-oxidation of the catalyst bulk proceed at different rates. In this work we investigated the evolution of the bulk structure of MoO_3, in combination with the catalytic activity under the reaction conditions of propene oxidation by oxygen. In order to reveal structure-reactivity relationships for MoO_3, this study focused on two characteristic features. First, the onset temperature of the oxidation of propene was correlated to changes in the molybdenum average valence and the bulk structure of MoO_3. Second, the nature of the structural defects induced in the layer structure of MoO_3 under reaction conditions was elucidated.

Onset of Reduction of MoO_3 in He, H_2, Propene, and Propene and Oxygen

From the data presented here and in previous reports it becomes evident, that the onset temperature for the reduction of MoO_3 in He (Figure 1), H_2,[13] propene,[10] and propene and oxygen (Figure 4) is approximately the same (≈ 620 K), and independent of the composition of the gas phase. Only in hydrogen, where the incorporation of hydrogen into the MoO_3 lattice facilitates the formation of MoO_2 product nuclei, is the onset temperature slightly shifted towards lower temperatures (≈ 600 K).[20] Apparently, the onset temperature for the reduction of MoO_3 coincides with the attainment of oxygen vacancies in the MoO_3 lattice with sufficient mobility. Only when the molybdenum-oxygen bonds in the MoO_3 lattice are weakened, and the oxygen in the lattice is sufficiently mobile and can participate in oxidation reactions proceeding at the surface of the catalyst, can stoichiometric reduction of MoO_3 with hydrogen or propene take place. Moreover, the onset of the reduction of MoO_3 coincides with the onset of propene oxidation on this material. This holds for both reduction of MoO_3 in propene and for the reaction of propene and oxygen in the presence of MoO_3. Again, it seems that both partial and total oxidation of propene on MoO_3 require a certain mobility of the lattice oxygen of MoO_3 and the formation of partially reduced defects, in order to proceed. Abstraction of a proton from propene to form an allylic species is a necessary prerequisite for the oxidation of propene to proceed on MoO_3 and determines the rate of conversion of propene. However, catalytic activity of MoO_3 is observed only after the Mo−O bonds in the lattice have become sufficiently weak to permit defect formation and activation of oxygen from the gas phase.

Evolution of the Average Valence of MoO_3 under the Reaction Conditions

The degree of reduction and, hence, the degree of defects in MoO_3 under partial oxidation conditions, can be estimated from the average valence of the molybdenum oxide (Figure 5), obtained from comparing the Mo-*K* edge position to that of suitable references. At a temperature of about 620 K, slight reduction of the molybdenum oxide occurs (Figure 4), independent of the composition of the gas phase. This is in agreement with the proposition that in this temperature range the oxygen ions in the lattice are mobile enough to be exchanged with oxygen in the gas phase (in oxygen), or to participate in the oxidation of propene (propene and oxygen), resulting in partially reduced MoO_3. In the temperature range from about 620 K to about 720 K, this partially reduced MoO_3 is not completely reoxidized by the oxygen in the gas phase. This may be because of the different rates of reduction (release of oxygen from the bulk) and re-oxidation of the bulk, or because, within this temperature range, the shear-structure defects formed do not readily back-transform into oxygen vacancies that could diffuse through the bulk to the surface and be filled with oxygen from the gas phase.

At reaction temperatures above about 720 K, re-oxidation of the partially reduced MoO_3 occurs during the treatment of MoO_3 in oxygen, and in propene and oxygen (ratio of 1:5) (Figure 4). Conversely, during the reaction of propene and oxygen (ratio of 1:1 and 1:3), re-oxidation of molybdenum is not detected at reaction temperatures above about 720 K. Apparently, at these ratios, the reducing potential of the gas phase with respect to the MoO_3 bulk is still too high to allow reoxidation of the molybdenum oxide.

Evidently, the ability of the atmosphere to reduce or oxidize the bulk material depends not only on the presence of oxygen in the gas phase, but also on the ratio of the reductant (propene) and the oxidant (oxygen). With an increasing concentration of oxygen, the reducing potential of the gas phase decreases until the partially reduced molybdenum oxide is reoxidized at temperatures above about 720 K.

Bulk Structural Evolution of MoO_3 under the Reaction Conditions

During the treatment of MoO_3 in oxygen or during the TPR in propene and oxygen, MoO_3 remains the only crystalline phase detected. In the temperature-programmed experiments, the evolution of the lattice parameters of MoO_3 is dominated by the anisotropic thermal expansion of MoO_3.[10] Therefore, the analysis described focused on integrated intensities and apparent crystallite sizes calculated for selected *hkl* reflections. The non-uniform behavior of the ratios of integrated intensities and apparent crystallite sizes (i.e. integral breadth) at temperatures above about 620 K (Figure 2 and Figure 3) indicates the formation of characteristic defects in the parent layer structure of MoO_3 without resulting in a long-range ordered separate phase under these reaction conditions. On the basis of our previous results on the reduction of MoO_3 in propene,[10] we suggest that the structure of molybdenum trioxide under propene oxidation reaction conditions corresponds to a defect-rich MoO_3 containing "$Mo_{18}O_{52}$" type defects. The close relationship between the structures of MoO_3 and $Mo_{18}O_{52}$ (Figure 8) facilitates the formation of "$Mo_{18}O_{52}$" type defects under these reaction conditions. Conversely, formation of other partially reduced molybdenum oxides that also contain shear-structures or tetrahedrally coordinated Mo, would require massive restructuring. Hence, they are less probable intermediates or structures formed at temperatures below 700 K. Therefore, the deviations observed in the ratios of integrated intensities (*h0l* > *hk0*, *hkl*) and apparent crystallite sizes, and the increase of strain in the MoO_3 lattice at temperatures above about 620 K, are caused by the formation of shear-structural defects (e.g. Wadsley defects) in the layer structure of MoO_3 under the reaction conditions (Figure 2 and Figure 3). In future work, these characteristic deviations may serve as starting points for a detailed investigation of the structural relationships between MoO_3 and $Mo_{18}O_{52}$, and of the effects of a transition between the two structures on the XRD patterns measured under reaction conditions.

The number of "$Mo_{18}O_{52}$" type defects formed cannot readily be estimated from the effect on the Fourier transform of the Mo-*K* edge XAFS measured under reaction conditions. A comparison of the radial distribution functions of MoO_3 and $Mo_{18}O_{52}$ for a 1 nm cluster (Figure 9) indicates that because of the large number of slightly different distances in the structure of $Mo_{18}O_{52}$, the magnitude of the Fourier transform of $Mo_{18}O_{52}$ is considerably smaller than that of MoO_3. Hence, even major fractions of $Mo_{18}O_{52}$ in MoO_3 may hardly be noticed from changes in the MoO_3 Fourier transform (Figure 10). Thus, the Mo-*K* XAFS spectra of MoO_3 under the reaction conditions correspond largely to that of pure defect-free MoO_3 (Figure 7) at elevated temperatures. The considerable number of defects in the MoO_3 structure (≈ 25% as estimated from the average Mo valence) is only accessible from their second order influence on the structural parameters, as obtained from an XAFS refinement of a MoO_3 model structure to the spectra of MoO_3 under reaction conditions (Figure 11).

Simulating the effect of the presence of "$Mo_{18}O_{52}$" in MoO_3 by calculating XAFS functions that correspond to mixtures of these two oxides, resulted in characteristic deviations in the XAFS fit parameters obtained for MoO_3 [i.e. increase in the Debye temperatures, and increase and decrease in the Mo−O distances in the 1st coordination shell, Figure 12, part (a) and Figure 13]. For the experimental spectra measured under the reaction conditions, at temperatures below about 620 K, the evolution of the XAFS fit parameters is dominated by the regular effect of the increasing reaction temperature [i.e. decreasing Debye temperatures and slightly increasing Mo−O distances, Figure 12, part (b) and Figure 14]. However, at temperatures above about 620 K, the oxygen Debye temperatures increase drastically, while the Mo−O distances in the 1st coordination shell exhibit a characteristic pattern of increasing and decreasing distances. The deviations observed in the XAFS fit parameters obtained for MoO_3 under reaction conditions at temperatures above about 620 K are similar to those obtained for the analysis of the mixtures of MoO_3 and $Mo_{18}O_{52}$. Therefore, the XAFS analysis of the Mo-*K* edge spectra measured under the reaction conditions corroborates the formation of "$Mo_{18}O_{52}$" type defects in the layer structure of MoO_3 during oxidation of propene at temperatures below 720 K.

Regarding the evolution of the bulk structure of MoO_3 in a reducing atmosphere of propene and oxygen (ratio of 1:1) at temperatures above 720 K, two possibilities with respect to the formation of oxygen vacancies can be envisioned. First, the "$Mo_{18}O_{52}$" type defects in the structure vanish at the expense of an increasing number of free oxygen vacancies in the MoO_3 structure. This would result in an average valence below 6.0 and an overall structure of the material close to that of MoO_3. Second, the "$Mo_{18}O_{52}$" type defects persist even at higher temperatures, resulting in an average valence below 6.0 and a disturbed bulk structure of MoO_3. The experimental data shown corroborate the second possibility (Figure 5, Figure 12, and Figure 13). Apparently, this very dynamic system under these reaction conditions is not governed by the energy necessary to break up the "$Mo_{18}O_{52}$" type defects and to form vacancies that can be filled with gas phase oxygen. Instead, the density of vacancies in the MoO_3 layer structure, resulting from the ratio of the rate of reduction of the MoO_3 lattice by propene and the rate of re-oxidation by gas phase oxygen, energetically favors the shear-structure defects, rather than the free oxygen vacancies.[21,22] Only at an increased oxygen partial pressure and temperatures above about 720 K, is the rate of re-oxidation of the MoO_3 lattice sufficient to allow the release of oxygen vacancies from the shear-structure de-

fects and, subsequently, filling of the oxygen vacancies by gas phase oxygen.

A schematic model for the behavior of MoO_3 under propene oxidation conditions is depicted in Figure 15.

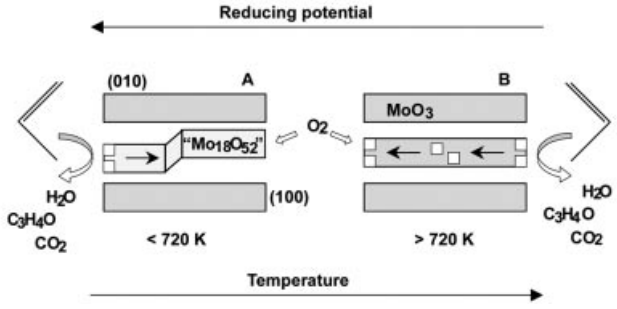

Figure 15. Schematic representation of the structure of MoO_3 under the reaction conditions (propene and oxygen), as a function of temperature and reducing potential of the gas phase. A) Below 720 K, **or** in a reducing gas phase. B) Above 720 K, **and** in an oxidizing gas phase. "$Mo_{18}O_{52}$" refers to crystallographic-shear type defects in the MoO_3 structure (squares indicate oxygen vacancies)

Oxygen vacancies are generated mostly at the side facets of the MoO_3 layer structure and can diffuse easily along the [100] or the [001] direction into the bulk.[23–26] Evidently, both reaction temperature and the reducing potential of the gas phase influence the bulk structure of the molybdenum oxide material under reaction conditions. By varying the reducing potential in the gas phase, the degree of reduction of the MoO_3 bulk can be adjusted. If the gas phase becomes oxidizing with respect to the bulk, at temperatures above about 720 K re-oxidation of the "$Mo_{18}O_{52}$" type defects in the MoO_3 layer structure takes place (B in Figure 15). Conversely, under a reducing atmosphere with respect to the MoO_3 bulk, "$Mo_{18}O_{52}$" type defects persist in the MoO_3 structure and the material is not completely reoxidized at elevated temperatures (A in Figure 15).

Evidently, under propene oxidation reaction conditions, the structure of the molybdenum oxide catalyst is not identical to that of the initial MoO_3. Rather, given the oxidation and reduction kinetics of molybdenum oxides at temperatures below about 720 K, the material corresponds to partially reduced metastable MoO_3 with a considerable number of "$Mo_{18}O_{52}$" type defects in the parent layer structure. From Figure 6 it can be seen that the catalytically most active and selective molybdenum oxide phase for propene oxidation to form acrolein develops under the reaction conditions. Possibly, a certain number of "$Mo_{18}O_{52}$" type defects have to be present in the bulk structure of MoO_3 to result in an improved selectivity in the partial oxidation of propene in the presence of MoO_3. The minor total oxidation activity at temperatures below about 600 K (Figure 6), which is not accompanied by a change in the average valence of the molybdenum oxide, may be assigned to adsorbed oxygen species.[27] However, a detailed analysis of the effect of oxygen partial pressure and temperature on the reactivity and selectivity of MoO_3 is not the subject of this report and shall be pursued in future studies. Furthermore, molybdenum trioxide obtained by various preparation routes will be investigated to elucidate the dependence of the defect type and the catalytic properties on the preparation conditions. In order to obtain more active and selective molybdenum oxide phases (e.g. Mo_5O_{14}), ternary oxides such as mixed molybdenum vanadium oxides are needed. It has to be clarified if these oxides need to be prepared, or if they can be obtained as binary molybdenum oxides by careful tailoring of the preparation conditions.

Many of the attempts to reveal the catalytic properties of MoO_3 described in the literature are restricted to "post-mortem" investigations, or studies on stoichiometric reactions involving molybdenum oxides and, for instance, oxidation by oxygen, or reduction by hydrogen or propene. Those investigations are valuable to elucidate the structural evolution of the material under noncatalytic conditions. Our previous investigations on the reduction and re-oxidation of MoO_3 allowed us to interpret the structural changes described here. However, only investigating the catalyst under reaction conditions (in situ) employing the modern in situ techniques available will eventually result in a complete description of the evolution of the bulk structure of the catalytically relevant material.

Naturally, an investigation of the evolution of the bulk structure of MoO_3 under reaction conditions cannot provide information on the individual steps of the partial oxidation of propene proceeding on the surface of the molybdenum oxide material used. However, while studying these surface reaction steps on defined model systems such as thin films or molecular molybdenum oxides, one needs to be aware of the importance of the bulk structure for the catalytic properties of a "real" heterogeneous catalyst. Attempting to access the reactivity of individual molybdenum oxide polyhedra, in order to model partial oxidation reactions proceeding on the surface of a bulk molybdenum oxide catalyst, requires taking into account the paramount role of the underlying bulk structure of the catalyst. By neglecting either the bulk or the surface, all the properties essential for the material to function as a heterogeneous catalyst cannot be comprehended and, hence, any attempts to design an improved catalyst based on this incomplete picture will fail. Eventually, a rational design of a most active heterogeneous catalyst will only be possible if both the structure and reactions of the surface, and the structure and reactions of the bulk are adequately understood and considered.

Conclusion

In this work we presented investigations on the evolution of characteristic defects in the bulk structure of MoO_3 under propene oxidation conditions using in situ X-ray absorption spectroscopy and X-ray diffraction. Under the reaction conditions employed (273 K to 773 K, and propene to oxygen ratios from 1:1 to 1:5), MoO_3 remains the only crystalline phase detected by XRD. The onset temperature for the temperature-programmed reaction of propene and oxygen in the presence of MoO_3 coincides with the onset

of the reduction of MoO_3 in He, H_2, or propene ($\approx$ 620 K). Thus, the weakening of Mo−O bonds in MoO_3, the sufficient mobility of oxygen ions, and the formation of defects are essential for the reduction of MoO_3 and for its function as a heterogeneous catalyst.

Various in situ experiments indicate that the structural evolution of MoO_3 during the TPR, reduction, and treatment in He is surprisingly similar. At temperatures below about 720 K, and independent of the atmosphere used, partial reduction of MoO_3 is observed, resulting in the formation of "$Mo_{18}O_{52}$" type defects in the bulk structure. At temperatures above about 720 K, and in oxygen or in an oxidizing atmosphere (sufficiently low propene to oxygen ratio), the "$Mo_{18}O_{52}$" type defects are reoxidized to MoO_3. Evidently, the catalytically active molybdenum oxide phase under partial oxidation conditions at temperatures below 720 K does not correspond to the original MoO_3 possessing the undisturbed ideal layer structure of orthorhombic α-MoO_3. Instead, at these temperatures, the catalytically active phase, which is partially reduced and possesses a large number of "$Mo_{18}O_{52}$" type defects (crystallographic-shear structures) in the layer structure of MoO_3, develops under reaction conditions.

The results presented clearly show the necessity and the great potential for bulk structural investigations of heterogeneous catalysts under reaction conditions. Evidently, the bulk structure and particularly the type and number of defects in the material ("real" structure) considerably affect the catalytic properties. Hence, in order to rationally design a most active heterogeneous catalyst, both the structure and reactions of the surface, and the structure, defects, and reactions of the bulk need to be known in detail, and carefully considered.

Experimental Section

MoO_3 Preparation and Characterization

Molybdenum trioxide (MoO_3) was prepared by thermal decomposition of ammonium heptamolybdate (AHM), $(NH_4)_6Mo_7O_{24}{\cdot}4H_2O$[28] (Aldrich Co.), under a stream of synthetic air (room temp. − 773 K with 2 K/min, held for 2 h at 773 K). The phase purity of the compound obtained was verified by XRD. The molybdenum trioxide used in this study is identical to that used in ref. 10 and 11.[10,11]

X-ray Diffraction

In situ XRD experiments were performed on a STOE STADI P powder diffractometer equipped with a secondary monochromator (Cu-K_α radiation) and a scintillation counter operated in the stepping mode. The in situ cell consisted of a Bühler HDK S1 high temperature diffraction chamber. The gas phase composition at the cell outlet was analyzed on line with a Pfeiffer Prisma 200 quadropole mass spectrometer in the multiple ion detection mode. In situ XRD measurements were conducted under atmospheric pressure with flowing reactants ($\approx$ 100 mL/min). Details on the XRD setup used can be found elsewhere.[11] Crystallite sizes were calculated from the integral breadth of selected *hkl* reflections using the Scherrer formula.[29]

In situ X-ray Absorption Spectroscopy

For in situ XAS experiments, MoO_3 was mixed with boron nitride (ratio 1:4) and 37 mg of the mixture was pressed with a force of 1 ton into a 5 mm diameter self-supporting pellet. The absorption jump, $\Delta\mu x$, at the Mo-*K* edge was about 1.5. In situ XAS experiments were performed in transmission in a flow-reactor[30] at atmospheric pressure with flowing reactants ($\approx$ 30 mL/min). The gas phase composition at the cell outlet was continuously monitored using a mass spectrometer in the multiple ion detection mode (QMS200 from Pfeiffer). Further details about the experimental XAS set-up used can be found in ref.[11].

In situ transmission XAS experiments were performed at the Mo-*K* edge (19.999 keV) at beamline X1 at the Hamburg Synchrotron Radiation Laboratory, HASYLAB, using a Si(311) double crystal monochromator (measuring time about 4.5 min/scan). The storage ring operated at 4.4 GeV with injection currents of 150 mA. Time-resolved in situ XAS experiments were carried out at the Mo-*K* edge utilizing an energy-dispersive spectrometer (European Synchrotron Radiation Facility, ESRF, ID24[31]) equipped with a curved Si(111) polychromator in the transmission mode[32] (measuring time about 3 s/scan). The storage ring operated at 6.0 GeV with injection currents of 90 mA in the 16-bunch mode.

XAFS Data Analysis

X-ray absorption fine structure (XAFS) analysis was performed using the software package WinXAS v2.2,[33] following recommended procedures from the literature.[34] Background subtraction and normalization were carried out by fitting linear polynomials to the pre-edge and the post-edge region of an absorption spectrum. The Mo-*K* edge absorption threshold was determined from the first root in the first derivative of the near-edge region (XANES). Principal component analysis (PCA)[35] was used to identify the number and type of Mo oxide phases[10] present during the thermal treatment of MoO_3 under various atmospheres.

The X-ray absorption fine structure (EXAFS) $\chi(k)$ was extracted by using cubic splines to obtain a smooth atomic background, $\mu_0(k)$. The radial distribution function $FT[\chi(k)]$ was calculated by Fourier transformation of the k^3-weighted experimental $\chi(k)$ function, multiplied by a Bessel window, into the R space. EXAFS data analysis was performed using theoretical backscattering phases and amplitudes calculated with the ab initio multiple-scattering code FEFF7.[36] Single scattering and multiple scattering paths in the MoO_3 model structure were calculated up to 5.0 Å, with a lower limit of 2.0% in amplitude with respect to the strongest backscattering path. EXAFS refinements were performed in the *R* space to the magnitude and the imaginary part of a Fourier-transformed k^3-weighted experimental $\chi(k)$, by using the standard EXAFS formula (k range from 3.1 to 15.4 $Å^{-1}$, *R* range 0.9 to 4.1 Å).[37] Structural parameters that were determined by a least-squares EXAFS fit to the experimental spectra are (i) one E_0 shift for oxygen and molybdenum backscatterers, (ii) two Debye temperatures for oxygen and molybdenum backscatterers, (iii) distances of the single-scattering paths with an amplitude larger than 10% were allowed to vary, distances of multiple-scattering paths were correlated to the corresponding single-scattering paths, (iv) one third cumulant for all scattering paths. Coordination numbers (CN) were kept constant in the refinement.

Acknowledgments

The synchrotron radiation facilities HASYLAB, Hamburg, Germany, and ESRF, Grenoble, France, are acknowledged for provid-

ing beamtime for this work. TR thanks the Deutsche Forschungsgemeinschaft, DFG, for financial support (Habilitations-Stipendium). T. Neisius and O. Timpe are acknowledged for participating in the XAS experiments. The authors are grateful to Prof. R. Schlögl for many fruitful discussions and continuous support.

[1] B. Grzybowska-Swierkosz, *Topics in Catalysis* **2000**, *11/12*, 23−42.
[2] R. K. Grasselli, *Catalysis Today* **1999,** *49*, 141−153.
[3] J. Haber, E. Lalik, *Catalysis Today* **1997,** *33*, 119−137.
[4] M. M. Bettahar, G. Costentin, L. Savary, J. C. Lavalley, *Appl. Cat. A* **1996**, *145*, 1−48.
[5] B. Grzybowska, J. Haber, J. Janas, *J. Catal.* **1977**, *49*, 150−163.
[6] K. Brückmann, R. Grabowski, J. Haber, A. Mazurkiewicz, J. Sloczynski, T. Wiltowski, *J. Catal.* **1987**, *104*, 71−79.
[7] P. Mars, D. W. van Krevelen, *Chem. Ing. Sci.* **1954**, *3*, 41.
[8] L. D. Krenzke, G. W. Keulks, *J. Catal.* **1980**, *61*, 316−325.
[9] W. Ueda, Y. Moro-Oka, T. Ikawa, *J. Catal.* **1981**, *70*, 409−417.
[10] T. Ressler, J. Wienold, R. E. Jentoft, O. Timpe, T. Neisius, *J. Catal.* **2002**, *210*, 67−83.
[11] T. Ressler, R. E. Jentoft, J. Wienold, M. M. Günter, O. Timpe, *J. Phys. Chem. B* **2000**, *104*, 6360−6370.
[12] R. Schlögl, *Angew. Chem. Int. Ed. Engl.* **1993**, *32*, 381−383.
[13] T. Ressler, J. Wienold, R. E. Jentoft, T. Neisius, M. M. Günter, *Topics in Catalysis* **2002**, *18*, 45−42.
[14] T. Ressler, J. Wienold, R. E. Jentoft, O. Timpe, T. Neisius, *Solid State Communications* **2001**, *119*, 169.
[15] D. C. Koningsberger, B. L. Mojet, *Topics in Catalysis* **2000**, *10*, 3.
[16] G. K. Williamson, W. H. Hall, *Acta Metall* **1953**, *1*, 22.
[17] L. Kihlborg, *Ark. Kemi* **1963**, *21*, 357.
[18] L. Kihlborg, *Ark. Kemi* **1963**, *21*, 443.
[19] R. L. Smith, G. S. Rohrer, *J. Solid State Chem.* **1996**, *124*, 104−115.
[20] T. Ressler, J. Wienold, R. E. Jentoft, *Solid State Ionics* **2001**, *141−142*, 243−251.
[21] E. Broclawik, J. Haber, *J. Catal.* **1981**, *72*, 379−382.
[22] R. Tokarz−Sobieraj, K. Hermann, M. Witko, A. Blume, G. Mestl, R. Schlögl, *Surface Science* **2001**, *489*, 107−125.
[23] A. Guerrero-Ruiz, J. M. Blanco, M. Aguilar, I. Rodriguez-Ramos, J. L. G. Fierro, *J. Catal.* **1992**, *137*, 429−436.
[24] A. Guerrero-Ruiz, I. Rodriguez-Ramos, P. Ferreira-Aparicio, M. Abon, J. C. Volta, *Catalysis Today* **1996**, *32*, 223−227.
[25] N. Floquet, O. Bertrand, J. J. Heizmann, *Oxidation of Metals* **1992**, *37*, 253−280.
[26] P. A. Batist, C. J. Kapteijns, B. C. Lippens, G. C. A. Schuit, *J. Catal.* **1967**, *7*, 33−49.
[27] J. Haber, W. Turek, *J. Catal.* **2000**, *190*, 320−326.
[28] J. Wienold, R. E. Jentoft, T. Ressler, *Eur. J. Inorg. Chem.* **2002**, submitted.
[29] R. J. Matyi, L. H. Schwartz, J. B. Butt, *Catal. Rev. Sci. Eng.* **1987**, *29*, 41.
[30] Designed by M. Hagelstein, T. Neisius, et al.,((***Author: please list all authors)***) ESRF, France, in a collaborative effort with the Fritz−Haber-Institut, Berlin, Germany
[31] M. Hagelstein, A. San Miguel, A. Fontaine, J. Goulon, *J. de Physique IV* **1997**, *7*, C2−303.
[32] M. Hagelstein, C. Ferrero, U. Hatje, T. Ressler, W. Metz, *J. Synch. Rad.* **1995**, *2*, 174−179.
[33] T. Ressler, *J. Synch. Rad.* **1998**, *5*, 118−122.
[34] D. C. Koningsberger, R. Prins, *X-ray Absorption Spectroscopy, Chemical Analysis*, 92, Wiley, New York, **1988**.
[35] T. Ressler, J. Wong, J. Roos, I. L. Smith, *Environ. Sci. & Technol.* **2000**, *34*, 950−958.
[36] J. J. Rehr, C. H. Booth, F. Bridges, S. I. Zabinsky, *Phys. Rev. B* **1994**, *49*, 12347−12350.
[37] T. Ressler, S. L. Brock, J. Wong, S. L. Suib, *J. Phys. Chem. B* **1999**, *103*, 6407−6420.

Received June 21, 2002
[I02332]